DiVA
http://www.diva-portal.org

Postprint

This is the accepted version of a paper published in *Journal of Physics B: Atomic, Molecular and Optical Physics*. This paper has been peer-reviewed but does not include the final publisher proof-corrections or journal pagination.

Citation for the original published paper (version of record):

Zhaunerchyk, V., Mucke, M., Salen, P., vd Meulen, P., Kaminska, M. et al. (2013)
Using covariance mapping to investigate the dynamics of multi-photon ionization processes of Ne atoms exposed to X-FEL pulses.
*Journal of Physics B: Atomic, Molecular and Optical Physics*, 46(16 SI): 164034
http://dx.doi.org/10.1088/0953-4075/46/16/164034

Access to the published version may require subscription.

N.B. When citing this work, cite the original published paper.

Permanent link to this version:
http://urn.kb.se/resolve?urn=urn:nbn:se:uu:diva-210261

# Using Covariance Mapping to Investigate the Dynamics of Multi-Photon Ionization Processes of Ne Atoms Exposed to X-FEL Pulses

**V. Zhaunerchyk[1], M. Mucke[1], P. Salén[2], P. vd. Meulen[2], M. Kaminska[1,3], R.J. Squibb[1,4], L.J. Frasinski[4], M. Siano[4], J.H.D. Eland[1,5], P. Linusson[2], R.D. Thomas[2], M. Larsson[2], L. Foucar[6,7], J. Ullrich[8,9], K. Motomura[10], S. Mondal[10], K. Ueda[10], T. Osipov[11], L. Fang[11], B.F. Murphy[11], N. Berrah[11], C. Bostedt[12], J.D. Bozek[12], S. Schorb[12], M. Messerschmidt[12], J.M. Glownia[12], J.P. Cryan[12], R.N. Coffee[12], O. Takahashi[13], S. Wada[14], M.N. Piancastelli[1,15], R. Richter[16], K.C. Prince[16], and R. Feifel[1]**

[1]Department of Physics and Astronomy, Uppsala University, Sweden
[2]Department of Physics, AlbaNova University Center, Stockholm University, Sweden
[3]Institute of Physics, Jan Kochanowski University, Kielce, Poland
[4]Department of Physics, Imperial College London, United Kingdom
[5]Department of Chemistry, Oxford University, United Kingdom
[6]Advanced Study Group of the Max Planck Society, Hamburg, Germany
[7]Max Planck Institut für medizinische Forschung, Heidelberg, Germany
[8]Max Planck-Institut für Kernphysik, Heidelberg, Germany
[9]Physikalisch-Technische Bundesanstalt, Braunschweig, Germany
[10]Institute for Interdisciplinary Material Research, Tohoku University, Sendai, Japan
[11]Department of Physics, Western Michigan University, Kalamazoo, MI, USA
[12]SLAC National Accelerator Laboratory, Menlo Park, CA, USA
[13]Department of Chemistry, Hiroshima University, Japan
[14]Department of Physical Science, Hiroshima University, Japan
[15]Laboratoire de Chimie Physique, Matière et Rayonnement (LCPMR), UPMC, Université Paris 06, and CNRS (UMR7614), 75231 Paris Cedex 05, France
[16]Elettra-Sincrotrone Trieste, Trieste, Italy

**Abstract.** We report on a detailed investigation into the electron emission processes of Ne atoms exposed to intense femtosecond X-ray pulses provided by the Linac Coherent Light Source Free Electron Laser at Stanford. The covariance mapping technique is applied to analyze the data and the capability of this approach to disentangle both linear and non-linear correlation features which may be hidden on coincidence maps of the same data set is demonstrated. Different correction techniques which enable improvements on the quality of the spectral features extracted from the covariance maps are explored. Finally, a method for deriving characteristics of the X-ray FEL pulses based on covariance mapping in combination with model simulations is presented.

## 1. Introduction

Detailed investigations into non-linear X-ray interaction with matter, in particular multiple X-ray photon absorption of atoms and associated relaxation processes, has not been feasible until the advent of the world's first X-ray Free Electron Laser (FEL), the Linac Coherent Light Source (LCLS) at the SLAC National Accelerator Laboratory, Stanford [1]. The defining characteristics of the LCLS in the present context are the high photon flux density and the possibility to generate ultra-short X-ray pulses of a few femtosecond duration comparable to the Auger decay time. Due to these properties, the LCLS enables formation of exotic states of matter such as double vacancies in inner electronic shells denoted as Double Core Holes (DCHs) via sequential two X-ray photon absorption, in which absorption of the second X-ray photon occurs prior to the Auger decay of the first core hole. Recent X-ray Photoelectron Spectroscopy (XPS) experiments performed at the LCLS have demonstrated the capability of creating DCHs in this way both for atomic and molecular species [2, 3, 4, 5, 6].

A problematic aspect in identifying DCHs by means of conventional, single-channel detection schemes, such as XPS, is that non-linear spectral features often overlap with signals originating from shake processes associated with the dominant single ionization process. In principle, electron coincidence measurements would ease disentangling contributions from non-linear DCH processes as they, in contrast to shake-off electron emission, correlate to the main photoelectron line. However, due to the comparatively low LCLS pulse repetition rate, which is $60-120$ Hz, and the high pulse intensities, traditional coincidence detection schemes are not so practical, as they either require extraordinary long data acquisition times or lead to an overwhelming amount of accidental coincident events.

An alternative way of correlating photoionization products, within the conditions of more than one ionization event per laser pulse, relates to the statistical analysis technique called covariance mapping which was introduced to the field of photoionization by Frasinski and coworkers in 1989 [7]. This method implies analysis of Poisson statistical fluctuations in series of electron or ion spectra recorded on a shot-by-shot basis, where pairwise correlations between the charged particles detected can be revealed by calculating the covariance between the corresponding signals of the single-shot spectra. The covariance of two random variables is defined as

$$\mathrm{Cov}(X,Y) = \langle XY \rangle - \langle X \rangle \langle Y \rangle , \tag{1}$$

where $\langle ... \rangle$ denotes the average. The first term denotes the correlated product as frequently explored by traditional coincidence techniques, and the second term denotes the uncorrelated product representing, e.g., accidental coincidence events. By calculating the covariance for all possible pairs of, for instance, the particle kinetic energies, a two-dimensional covariance map is obtained. This literally means that the covariance map is found from equation (1) where input parameters $X$ and $Y$ represent series of photoionization spectra measured simultaneously by two different detection systems. In the case when only one detector is used, $X$ and $Y$ are the same and the calculated covariance map will be symmetric with respect to the main diagonal which corresponds to the variance.

The covariance mapping approach described by equation (1) relies on the photon flux to be stable. However, if this varies from shot to shot, artificial correlation features arise in the map. In this case, common variations of the signals may be induced by

intensity fluctuations of the ionizing source rather than by Poisson fluctuations of the statistical processes associated with the photoionization event. This issue can be relevant for the LCLS since it is operated as a so-called Self Amplified Spontaneous Emission (SASE) source [8] which starts up from noise and is characterized by fluctuating pulse intensities. To correct for this kind of artificial spectral contributions a so-called *partial* covariance mapping analysis can be employed where the fluctuations of the FEL intensity is taken into account on a shot-by-shot basis [9, 10]. The partial covariance is calculated as

$$\mathrm{Cov}_p(X,Y) = \mathrm{Cov}(X,Y) - \frac{\mathrm{Cov}(X,I)\mathrm{Cov}(Y,I)}{\mathrm{Var}(I)}, \tag{2}$$

where $I$ denotes the pulse intensities measured for each laser shot.

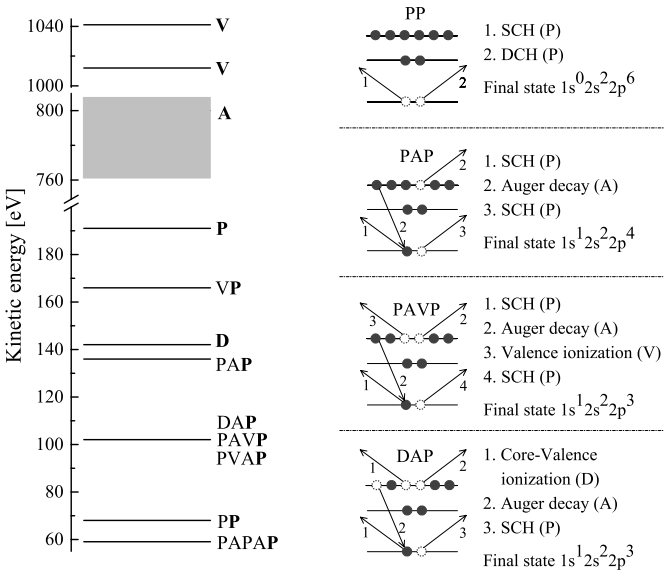


**Figure 1.** Multi-photon processes in Ne and associated electron kinetic energies. The left-hand diagram shows the kinetic energies of electrons created upon ionization by 1062 eV photons, labeled according to the chronological sequence of the following processes: core photoionization (P), valence photoionization (V), single photon core-valence double ionization (D) and Auger decay (A). Four crucial multi-photon processes are schematically presented in the right-hand diagram using the same notation. Arrows indicate the ejected electrons and are numbered in chronological order.

In the present work we explore the capability of the covariance mapping approach and present an elaborate study where this analysis method is applied to photoionized Ne atoms exposed to highly intense X-FEL radiation, expanding on our very recent comprehensive work on this subject [10]. We aim at presenting more detailed physical results deduced from the covariance map of Ne including some technical and computational details which have not been presented so far. Furthermore, we also present numerical results from modeling the time evolution of single and multi-photon processes leading to the ejection of core (P), Auger (A) or valence (V) electrons such as PAP, PP, VP, PAVP, PVAP and PAPAP, which are schematically illustrated in

figure 1. The model results will be compared directly with our experimental data analyzed by the technique of covariance mapping, giving deeper insights into these processes and the properties of the LCLS pulses.

## 2. Experimental details

The experiment was performed at the Atomic, Molecular and Optical (AMO) science instrument of the LCLS at the SLAC National Accelerator Laboratory, Stanford [11]. The LCLS was operated with ∼8 fs electron bunches carrying a charge of 40 pC and generating about 0.2 mJ optical pulses at the central photon energy of ∼1062 eV. Four gas detectors, which are routinely available at the AMO instrument, were used to monitor the LCLS pulse energy on a shot-by-shot basis. As the LCLS is operated in the SASE mode, the X-ray pulse energy is found to vary about 15%.

A pulsed beam of Ne gas crossed the X-ray beam at the light-matter interaction point of the High-Field Physics (HFP) chamber of the AMO. The optical pulses were focused with a pair of elliptically bent Kirkpatrick-Baez mirrors, and the FWHM diameter of the focused beam is estimated to be ∼1.4 $\mu$m or better which provides peak intensities up to about $1.5{\cdot}10^{17}$ W/cm$^2$, assuming a transmission of the AMO beam line optics of about 15% [5]. The electron kinetic energies were analyzed by means of a long Time-Of-Flight (TOF) Magnetic Bottle electron Spectrometer (MBS), custom-made for the present purpose and fitted to HFP of AMO. This spectrometer is characterized by a high collection efficiency of more than 90% of the whole $4\pi$ solid angle, implying a total collection-detection efficiency for single electrons of $\eta \approx 50\%$. A more detailed description of this spectrometer can be found in Ref. [12].

## 3. Numerical model

The model for calculating the signal strength of different ionization channels relevant to the present study is based on the work of Rohringer and Santra [13]. It uses coupled rate equations to calculate the population probability of a certain state of an atom exposed to a specific X-ray pulse as a function of time. The total probability for a particular transition is then given by calculating the probability for ionizing that state and integrated over the X-ray pulse duration. The photon flux, $j$, of the pulse as a function of time is defined by the X-ray pulse length, the beam radius and the number of photons in the pulse. Here a Gaussian temporal shape and a cylindrical spatial intensity profile is assumed, where the latter is constant as a function of distance from the center of the beam and drops to zero above the beam radius.

In the present case we assume a Ne atom initially in its neutral ground state with a population probability $P_0(0)$=1. We use the photoionization cross-sections $\sigma_v$=$9.8{\cdot}10^{-25}$ m$^2$ for the removal of a valence electron, and $\sigma_{1s^2\rightarrow 1s^1}$=$1.9{\cdot}10^{-23}$ m$^2$ for the removal of a $1s$ core electron [14]. Hence the ground state population probability as a function of time, $t$, can be described by:

$$\frac{dP_0(t)}{dt} = -\left(\sigma_{1s^2\rightarrow 1s^1} + \sigma_v\right) P_0\left(t\right) j\left(t\right). \tag{3}$$

In a similar way the population probability for the Ne atom with a single core hole (SCH), $P_{1s^1}$, is described by:

$$\frac{dP(t)_{1s^1}}{dt} = \sigma_{1s^2\rightarrow 1s^1} j(t) P_0(t) - \sigma_{1s^1\rightarrow 1s^0} j(t) P_{1s^1}(t) -$$

$$\sigma_v j(t) P_{1s^1}(t) - \Gamma_{1s^1}(\text{Auger}) P_{1s^1}(t), \tag{4}$$

where $\Gamma_{1s^1}(\text{Auger}) = 4.2{\cdot}10^{14}$ s$^{-1}$ is the Auger decay rate for a Ne atom with one $1s$ electron removed and $\sigma_{1s^1 \to 1s^0} = 9.5{\cdot}10^{-24}$ m$^2$ is the cross-section for ionizing the second $1s$ electron to form a DCH state. The latter is approximated as half the cross-section for ionizing the first $1s$ electron based on simple statistical arguments (one $1s$ electron compared with two). The Auger decay rate for a double core hole was set to $3 \times \Gamma_{1s^1}$ [15].

Using the same principle many more important states can be included. Knowing the population probability for the states as a function of time allows us to calculate the probability for a specific process by integrating the probability for its final transition over the X-ray pulse length. For example, the probability for a two-photon absorption process forming a DCH state is given by:

$$P_{1s^0} = \int \sigma_{1s^1 \to 1s^0} j(t) P_{1s^1}(t) dt. \tag{5}$$

In this way the relative intensities of different states can be modeled. In the present model the shake-off processes and double Auger decays are not considered.

## 4. Data treatment

Electron TOF spectra were recorded for every LCLS shot containing up to $\sim$ 50 photoelectrons. The spectra were converted to electron kinetic energies, $E_{kin}$, according to

$$E_{kin} = \frac{D_0^2}{(t - t_0)^2} + E_0, \tag{6}$$

where $t$ denotes TOF and $D_0$, $t_0$ and $E_0$ are conversion and calibration factors which were determined for the present experiment to be 3739 ns$\sqrt{\text{eV}}$, 3920.4 ns, and 0 eV, respectively. The $E_{kin} < 10$ eV region is not considered here as these signals might be strongly affected by secondary electrons from undesired scattering processes. The data were converted according to the positions of the main SCH peaks of Ne and $N_2$, the latter present in the chamber as a residual gas. A total number of $N_{shots} = 510\,576$ LCLS shots, which corresponds to a data acquisition time of about 80 minutes, were used to evaluate the covariance signals. The two-dimensional map of Ne electrons obtained for the large kinetic energy range of 10$-$1200 eV is presented in figure 2(a). Specific parts of this map which reflect correlations of several $K$-shell electrons or correlations of $K$-shell electrons with valence electrons are depicted in figure 2(b) and figure 2(c), respectively. Furthermore, figure 2(d) shows, for comparison, a raw form of coincidence evaluation ($\langle XY \rangle$=Coinc$(X,Y)N_{shots}$) of the experimental data for the energy region corresponding to electrons emitted from inner shells (cf. figure 2(b)), which elucidates the capability of the covariance mapping approach to eliminate accidental correlations and to reveal otherwise hidden structures. For instance, in figure 2(b) one can see a distinct line (labeled 5) perpendicular to the diagonal of $E_{kin}^{(1)}$=$E_{kin}^{(2)}$ which corresponds to the kinetic energy sum $E_{kin}^{(1)}$+$E_{kin}^{(2)}$=143 eV and which is not discernible in the coincidence map of panel (d) of this figure. Also, figure 2(d) shows an almost continuous correlation of any electron with $E_{kin}^{(1,2)}$=194 eV, while in the covariance map (cf. figure 2(b)) well separated islands are revealed. We note that other means than the present covariance approach (cf. Eq. 1 above) can be used

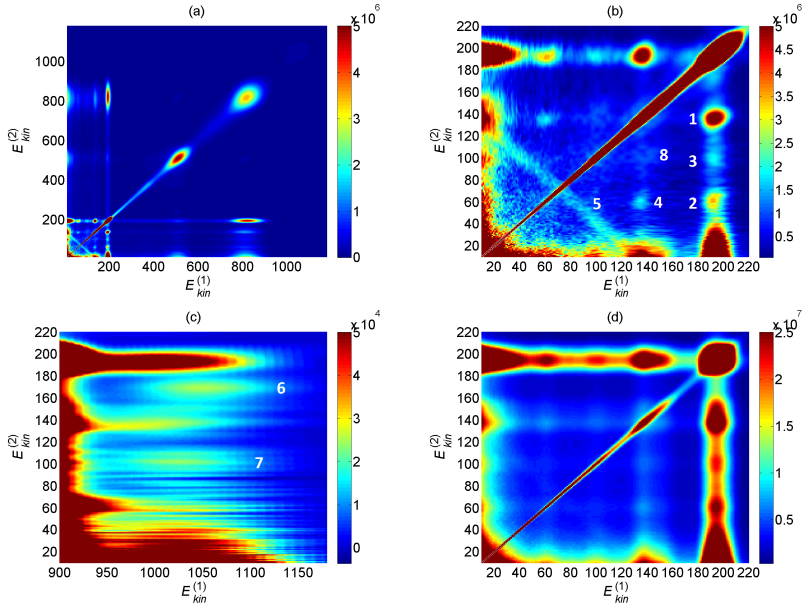


**Figure 2.** (a) Covariance map of Ne atoms obtained for > 500 000 LCLS shots at the central photon energy of ∼ 1062 eV; panels (b) and (c) show details of panel (a) emphasizing pair-correlations of several $K$-shell electrons or $K$-shell electrons with valence electrons, respectively; panel (d) shows a coincidence evaluation ($< XY >$=Coinc$(X,Y)N_{shots}$) of the experimental data for the energy region corresponding to electrons emitted from inner shells.

to correct for false coincidences dominating figure 2(d) which can result in similar drastic improvements of the data quality as demonstrated here. The results presented in figure 2 were obtained with the partial covariance mapping approach (equation 2). Since the LCLS light intensity fluctuated only within the range of 15% for the present recordings, our analysis showed that under such conditions this correction is moderate.

To obtain the results presented in figure 2 the raw electron kinetic energy spectra were corrected with respect to the photon energy jitter and to the electronic noise of the detector, which included contributions from reflections in the high voltage cables of the detector, and were subsequently deconvoluted to improve the overall quality of the spectral features. Figure 3 demonstrates a sequence of these data treatments applied to the inner-shell electron kinetic energy region and and shows their individual effects on the covariance map studied. As a control, figure 3(a) presents this covariance map based on the raw data before any data correction was applied. The first correction applied to the data aimed at discriminating unwanted signals such as reflections in cables and electronic noise, and the outcome of this operation is displayed in figure 3(b). This correction implies that all signals which were below the discrimination level were set to zero, while other signals were unaffected. As one can see, the noise discrimination of the signal removes false correlations in particular those which are associated with reflections in the cables. The second correction applied took the jitter in photon energy into account. This was achieved by shifting the entire single-shot energy spectra by a value which corresponds to the deviation from the mean photon energy value; the effect of this correction is displayed in figure 3(c). The photon

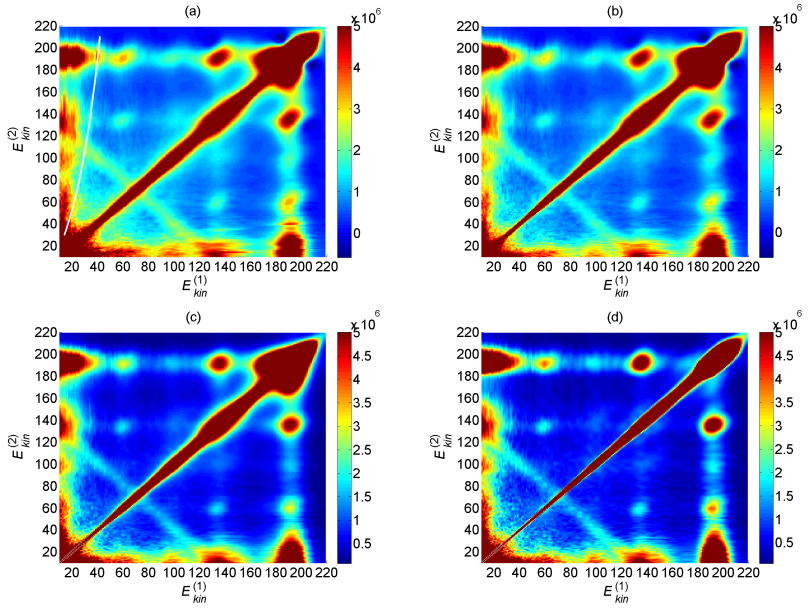


**Figure 3.** Covariance maps of neon for the electron kinetic energy range of 10−220 eV obtained from: (a) Raw experimental data; the white curve can be traced back to an additional signal associated with a reflection in the high voltage cables of the detector appearing in the TOF spectra 320 ns away from every electron peak. (b) Discriminated data. (c) Energy shifted data compensating for the photon energy jitter. (d) Fourier deconvoluted data (cf. figure 2(b)).

energy at every LCLS shot was derived from the radiofrequency Linac electron beam parameters.

To improve the spectral quality further every measured TOF spectrum, $W_{meas}$, was deconvoluted before converting it to the kinetic energy scale by means of a Fourier transform technique according to

$$W = \mathrm{F}^{-1}\left(\frac{\mathrm{F}(W_{meas})}{\mathrm{F}(W_{1e})}\right) \tag{7}$$

where $W_{1e}$ denotes a single electron waveform and F and $\mathrm{F}^{-1}$ denote the Fourier transformation and its inverse operation, respectively. $W_{1e}$ was derived from those TOF spectra where the electron count rate was low enough not to contain overlapping signals. For further details of such data deconvolution see Ref. [16]. We note that after this data correction was applied, the resolution of features appearing on the covariance map is still inferior compared to what is expected from the intrinsic resolution of our spectrometer which is around $\Delta E/E \approx 2\%$. This suggests that defining factors for the resolution of signals associated with photoelectrons at the present time are the light source properties such as the spikiness of the LCLS pulses due to its SASE nature, implying that the pulses most likely consist of several spikes of somewhat different photon energies.

## 5. Results and Discussion

Figure 2 shows distinct spectral features which are revealed by covariance mapping and which can be associated with pairwise correlations of the electrons formed upon

sequential X-ray multi-photon absorption by Ne atoms. The map exhibits strong signal intensities located along the diagonal, $E_{kin}^{(1)}$=$E_{kin}^{(2)}$, which represents the variance or the strength of the individual electron peaks which are typically measured with conventional electron spectroscopy techniques. The strongest off-diagonal feature, labeled in figure 2(b) as correlation island 1, corresponds to a PAP process (cf. figure 1). The presence of this island is expected since core-ionized Ne atoms have an Auger decay lifetime of ∼2.4 fs [15], while the LCLS pulse duration was ∼8 fs, which implies that there is a significant probability for the core-ionized system to decay by Auger electron emission before the second X-ray photon is absorbed. The competing two-photon formation of DCHs requires removal of two core electrons before the Auger decay sets in, and, within the present experimental conditions, it is expected to be less probable than the PAP sequence. Within the given pulse duration, it is also possible that a Ne atom may sequentially absorb three X-ray photons where each absorption step is followed by Auger decay giving rise to consecutive PAPAP. We find that the feature labeled correlation island 2 in figure 2(b) may originate both from such a PAPAP sequence and from PP emission associated with DCH formation, while island 4 can only be due to PAPAP. This offers the possibility to extract the relative population of the DCH state, $\tilde{V}_{\rm PP}$, as $\tilde{V}_{\rm PP}$=$\tilde{V}_4$-$\tilde{V}_2$, where $\tilde{V}_4$ and $\tilde{V}_2$ represent the integrated volumes of islands 4 and 2 derived from figure 2(b).

Figure 2(c) reveals another well separated feature denoted as island 6, and which shows the contribution from a VP process. Feature 5, located along the line of $E_{kin}^{(1)}$+$E_{kin}^{(2)}$ = 143 eV, corresponds to a single photon double ionization event which leaves the Ne atom with two electronic vacancies, one in the core and the other one in the valence shells (cf. figure 1: "D" process) [17, 18]. In this process the two emitted electrons share the available energy randomly following a "U"-shaped distribution which favors the case when one of the two electrons receives a major part of the energy. The location of this feature implies simultaneous ionization of the $1s$ and $2p$ orbitals. There is also a weak, washed-out feature denoted in figure 2(b) as island 8 which might be due to a two photon process of DAP type in which the initial single-photon core-valence double ionization is followed by an A and P process. The DAP process should in principle manifest itself on the covariance map as a continuous line with $E_{kin}^{(1)}$ ranging from 0 to 143 eV and with $E_{kin}^{(2)} \approx$ 102 eV. However, since the D process favors production of 143 eV electrons, this part of the weak feature is primarily discernible as an island.

To determine the nature of island 3 is not so straightforward. It could be either due to a three photon process of the PAVP or PVAP type, or a two-photon PAP(sat) process involving satellite electron emission of shake-up type associated with the second photoelectron of the PAP sequence. The location of island 3 disagrees by ≈ 10 eV with the theoretical predictions for the PAP(sat) process (Table 1). However, if we assume that correlation island 7 in figure 2(c) is a signature of the PAVP and PVAP processes, then $\tilde{V}_7$<<$\tilde{V}_3$ gives further support to assign island 3 to the PAP(sat) process. All feature assignments are summarized in Table 1.

To shed more light onto the dynamics of single and multi-photon processes we employed the numerical model outlined in Sec. 3 and compared the outcome with our experimental results. The intensities of the different processes in the model calculations were obtained as discussed earlier in the context of equation 5, while the experimental values were extracted by integrating the volume of the corresponding island on the covariance map, $\tilde{V}$. The values $\tilde{V}$ deduced from the map were corrected

**Table 1.** Location of the correlation islands deduced from figure 2. Their assignments are confirmed by comparison with theoretical predictions. The $E_{kin}$ values given correspond to specific sequences of the multi-ionization processes as labeled in bold in the third column. To denote the Ne $1s^r2s^t2p^k$ electron configurations the notation $rtk$ is used.

| | $E_{kin}$, eV | Assignment | Theory[a] | Theory[b] | Transition |
|---|---|---|---|---|---|
| Island 1 | (192±7,136±6) | **PAP** | (192[c],132) | (191,136) | $(226 \rightarrow 126, 224 \rightarrow 124)$ |
| | | | (192[c],139) | (191,139) | $(226 \rightarrow 126, 215 \rightarrow 115)$ |
| | | | (192[c],-) | (191,137) | $(226 \rightarrow 126, 206 \rightarrow 106)$ |
| Island 2 | (191±7,60±4) | **PP** | (192[c],69) | (191,68) | $(226 \rightarrow 126, 126 \rightarrow 026)$ |
| Island 3 | (193±7,95±7) | **PAP(sat)** | (192[c],-) | (191,78) | $(226 \rightarrow 126, 224 \rightarrow 1231$[d]$)$ |
| | | **PAP(sat)** | (192[c],-) | (191,85) | $(226 \rightarrow 126, 215 \rightarrow 1141$[d]$)$ |
| | | **PAP(sat)** | (192[c],-) | (191,80) | $(226 \rightarrow 126, 206 \rightarrow 1051$[d]$)$ |
| | | **PAVP** | (192[c],103) | (191,102) | $(226 \rightarrow 126, 223 \rightarrow 123)$ |
| | | **PAVP** | (192[c],107) | (191,105) | $(226 \rightarrow 126, 214 \rightarrow 114)$ |
| | | **PAVP** | (192[c],105) | (191,104) | $(226 \rightarrow 126, 205 \rightarrow 105)$ |
| | | **PVAP** | (192[c],103) | (191,102) | $(226 \rightarrow 126, 223 \rightarrow 123)$ |
| | | **PVAP** | (192[c],107) | (191,105) | $(226 \rightarrow 126, 214 \rightarrow 114)$ |
| | | **PAVP** | (192[c],105) | (191,104) | $(226 \rightarrow 126, 205 \rightarrow 105)$ |
| Island 4 | (138±6,60±6) | PA**P**A**P** | (132,61) | (136,59) | $(224 \rightarrow 124, 222 \rightarrow 122)$ |
| | | PA**P**A**P** | (139,70) | (139,68) | $(215 \rightarrow 115, 213 \rightarrow 113)$ |
| | | PA**P**A**P** | (-,69) | (137,67) | $(206 \rightarrow 106, 204 \rightarrow 104)$ |
| Island 5 | $E^1_{kin}+E^2_{kin}$ =143±5 | **D** | ∼143[e] | ∼142[f] | $(226 \rightarrow 125)$ |
| Island 6 | (1049±15,169±5) | **VP** | (1040[c],167) | (1041,166) | $(226 \rightarrow 225, 225 \rightarrow 125)$ |
| | | **VP** | (1013[g],-) | (1012,167) | $(226 \rightarrow 216, 216 \rightarrow 116)$ |
| Island 7 | (1024±15,103±4) | PA**VP** | (1000,103) | (999,102) | $(224 \rightarrow 223, 223 \rightarrow 123)$ |
| | | PA**VP** | (1004,107) | (1002,105) | $(215 \rightarrow 214, 214 \rightarrow 114)$ |
| | | PA**VP** | (-,105) | (1000,104) | $(206 \rightarrow 205, 205 \rightarrow 105)$ |
| | | P**V**A**P** | (1014,103) | (1016,102) | $(126 \rightarrow 125, 223 \rightarrow 123)$ |
| | | P**V**A**P** | (989,107) | (988,105) | $(126 \rightarrow 116, 214 \rightarrow 114)$ |
| Island 8 | (138±5,101±6) | **DAP** | (∼143,103) | (∼142,102) | $(226 \rightarrow 125, 223 \rightarrow 123)$ |

[a] Ref. [19].
[b] Ref. [20].
[c] experimental data from Ref. [21].
[d] the notation of $rtkl$ is used for $1s^r2s^t2p^k3s^l$.
[e] experimental data from Ref. [17].
[f] experimental data from Ref. [18].
[g] experimental data from Ref. [22].

for the drop of ≈ 50% in $\eta$ for electrons with $E_{kin}>$ 700 eV. The $\eta$ reduction was found by comparing the integrated intensities of Auger and $K$-shell photoelectrons. Since some of the model input parameters could not be determined very accurately, such as the pulse duration, the diameter of the focal spot size and the pulse energy, the simulations were consecutively performed for different sets of input parameters and the results obtained were compared to the experimental values deduced from the covariance maps. Note that the simulated intensity ratios depend on the pulse length and the peak intensity, where the latter is a function of the beam diameter and the pulse energy. Therefore the beam diameter was fixed at 1.4 $\mu$m FWHM and the peak intensity at a specific pulse length was varied by changing the pulse energy. With the four strongest islands under consideration, *viz.* the islands labeled 1, 2, 4, and SCH, it was not possible to entirely reconcile the model and the experimental results within a reasonable range of input parameters. However, considering only the non-linear

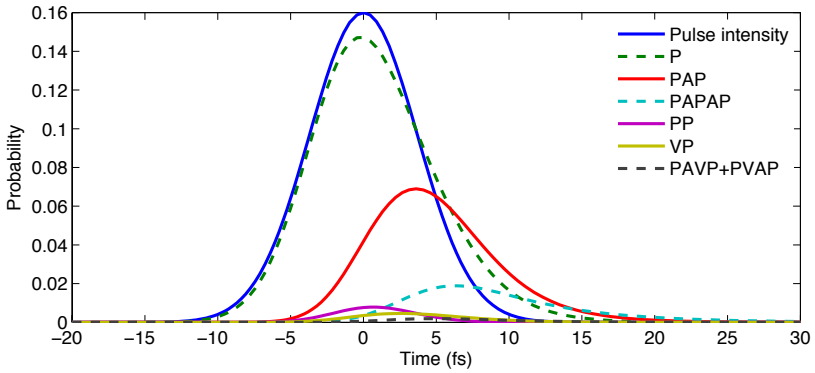


**Figure 4.** Evolution of linear and non-linear processes in time. As reference, the pulse intensity profile is shown in blue.

**Table 2.** Integrated intensities of our model calculations and our experimental results associated with different features of the covariance maps relative to the intensity of the feature associated with the PAP process. The experimental values were corrected for the collection-detection efficiency of the spectrometer used, taking into account a decrease of about 50% for energetic valence and Auger electrons.

| | Simulation | Covariance mapping |
|---|---|---|
| $\tilde{V}_{\mathrm{PA}}/\tilde{V}_{\mathrm{PAP}}$ | 2.9 | 3.1 |
| $\tilde{V}_{\mathrm{PP}}/\tilde{V}_{\mathrm{PAP}}$ | 0.28 | 0.28 |
| $\tilde{V}_{\mathrm{PAPAP}}/\tilde{V}_{\mathrm{PAP}}$ | 0.18 | 0.18 |
| $\tilde{V}_{\mathrm{VP}}/\tilde{V}_{\mathrm{PAP}}$ | $7.4{\cdot}10^{-2}$ | $4.3{\cdot}10^{-2}$ |
| $(\tilde{V}_{\mathrm{PAVP}}+\tilde{V}_{\mathrm{PVAP}})/\tilde{V}_{\mathrm{PAP}}$ | $2.2{\cdot}10^{-2}$ | $1.6{\cdot}10^{-2}$ |

correlations, which are primarily reflected by islands 1, 2 and 4, it was possible to find a fairly good agreement for the following input parameters: pulse duration of 8.7 fs (FWHM), beam diameter of 1.4 $\mu$m (FWHM), and pulse energy of 17 $\mu$J. The time evolution of different processes deduced from the simulations with these X-ray pulse parameters are shown in figure 4.

The results of our model calculations are listed together with the corresponding experimental results in table 2, where the volume $\tilde{V}$ of the islands associated with the different processes are presented relative to the PAP process. The intensity ratio of the spectral features associated with the formation of P and PAP was estimated from the integrated volumes of the off-diagonal islands corresponding to **PA** and P**AP** electron correlations. These islands were chosen instead of the P and **PAP** features to avoid ambiguity in the $\eta$ value. In addition to that, to reduce possible contributions from other processes that can also contribute to these islands the corresponding $\tilde{V}$ values were found by integrating over the Auger electron region of $800 < E_{kin} < 820$ eV, where the processes of interest are expected to be dominant. As can be seen from table 2, the simulation results agree well with the experimentally deduced values. Since the simulated intensity ratios for the $\tilde{V}_{\mathrm{PP}}/\tilde{V}_{\mathrm{PAP}}$ and $\tilde{V}_{\mathrm{PAPAP}}/\tilde{V}_{\mathrm{PAP}}$ fit to the experimental values, also the $\tilde{V}_{\mathrm{PP}}/\tilde{V}_{\mathrm{PAPAP}}$ ratio fits to the experiment results. In the simulations the $\tilde{V}_{\mathrm{PP}}/\tilde{V}_{\mathrm{PAP}}$ ratio is mainly determined by the pulse duration since the involved

processes are both of the two-photon type. Consequently the pulse duration can initially be estimated from this ratio, and the peak intensity is subsequently adjusted to match the $\tilde{V}_{\mathrm{PAPAP}}/\tilde{V}_{\mathrm{PP}}$ ratio, which is sensitive to both the peak intensity and pulse duration. The weak sensitivity of two-photon processes to the peak intensity is discussed further in Ref. [16]. The derived pulse energy of 17 $\mu$J compares reasonably well with the expected value of 15% of 0.2 mJ bearing in mind that the peak intensity also depends quadratically on the beam diameter which was fixed. It also follows that the experimentally deduced $\tilde{V}$ values for the VP, PVAP and PAVP processes are lower compared with the model predictions. It might be that we have underestimated the reduction in $\eta$ for the valence electrons as we assume it to be the same as for the Auger electrons, even though they have $\approx$ 200 eV higher kinetic energy.

## 6. Conclusions

A detailed investigation into covariance mapping analysis of the electrons emitted by Ne atoms exposed to intense fs X-ray FEL pulses has been presented. The capability of the covariance mapping technique for disentangling correlating signals which are hidden on coincidence maps recorded under the same experimental conditions, *i.e.,* the tolerance of the covariance analysis to the high event count rate, has been elucidated. In particular it has been shown that the covariance mapping approach is very suitable for correlation experiments at FEL sources such as the LCLS, in which low pulse repetition rate demands relatively high ionization rates for good statistics measurements within the typical amount of beam time available. More specifically, with covariance mapping we have been able to disentangle several two-photon processes such as PAP, PP, PAP(sat) and VP, as well as the three-photon processes, PAVP, PVAP and PAPAP. We also found a moderate effect of the partial covariance mapping analysis (equation (2)) compared to when the pulse intensity fluctuations were not taken into account (equation (1)), which relates to comparatively weak fluctuations of the LCLS pulses energy at the level of 15%. Based on the widths of the measured photoelectron peaks we conclude that the limiting factor for the energy resolution is primarily determined by the properties of the light source. The intensities of the multi-photon processes deduced from the covariance maps have been compared to the results of numerical simulations to cooperate the assignments of the correlation islands. Furthermore, since the probability of multi-photon processes strongly depends on the properties of the X-ray pulses such as the intensity and the pulse duration, we showed that the covariance mapping analysis together with modeling can be an efficient tool to derive quantitative values for some X-ray pulse parameters. We note that these values cannot very accurately be obtained from the machine parameters and only under certain assumptions, *e.g.*, that the optical pulse duration equals the electron bunch length.

We are currently applying the covariance mapping technique to the analysis of multi-photon ionization processes in molecular systems, *e.g.,* $C_2H_2$ and $C_2H_6$, obtained at the LCLS, with the aim at disentangling the formation of single-site and two-site DCH states. We also work on the extension of the two-dimensional covariance mapping approach towards multiple dimensions including intensity fluctuations of the ionization source which will enable us to establish the correlations between three or even more charged particles.

## 7. Acknowledgments

This work has been financially supported by the Swedish Research Council, the Göran Gustafsson Foundation (UU/KTH), and the Knut and Alice Wallenberg Foundation, Sweden. MK thanks the Swedish Institute for financial support. LJF and RJS thank the EPSRC, UK (Grants No. EP/F021232/1, EP/F034601/1 and EP/I032517/1). KCP and RR acknowledge the MIUR, Italy (Grants No. FIRB-RBAP045JF2 and No. FIRB-RBAP06AWK3). KU and KM are grateful to MEXT for funding the X-ray Free Electron Laser Utilization Research Project and the X-ray Free Electron Laser Priority Strategy Program. SM is grateful to JSPS for financial support. NB, TO, LF, and BFM acknowledge financial support by the U.S. Department of Energy of Science, Basic Energy Science, Chemical, Geosciences, and Biological Divisions. MNP wishes to thank the French ANR (Agence Nationale de la Recherche) for partial support during her stay at LCLS. Portions of this research were carried out at the Linac Coherent Light Source (LCLS) at the SLAC National Accelerator Laboratory. LCLS is an Office of Science User Facility operated for the U.S. Department of Energy Office of Science by Stanford University.

## References

[1] Emma P *et al* 2010 *Nature Photonics* **4** 641.
[2] Young L *et al* 2010 *Nature* **466** 56.
[3] Hoener M *et al* 2010 *Phys. Rev. Lett.* **104** 253002.
[4] Fang L *et al* 2010 *Phys. Rev. Lett.* **105** 083005.
[5] Berrah N *et al* 2011 *Proc. Natl. Acad. Sci.* **108** 16912.
[6] Salen P *et al* 2012 *Phys. Rev. Lett.* **108** 153003.
[7] Frasinski L J*et al* 1989 *Science* **246** 1029.
[8] Emma P *et al* 2004 *Phys. Rev. Lett.* **92** 074801.
[9] Frasinski L J *et al* 1996 *J. Elect. Spect. Rel. Phen.* **79** 367.
[10] Frasinski L J *et al* (2013), submitted to Phys. Rev. Lett.
[11] Bozek J 2009 *Eur. Phys. J. Special Topics* **169** 129.
[12] Mucke M *et al.* (2013), unpublished.
[13] Rohringer N and Santra R 2007 *Phys. Rev. A* **76** 033416.
[14] Wuilleumier F and Krause M O 1974 *Phys. Rev. A* **10** 242.
[15] Inhester L *et al* 2012 *JCP* **136** 144304.
[16] "Double core hole formation in small molecules at the LCLS free electron laser" by Larsson M *et al* in this volume.
[17] Hikosaka Y *et al* 2006 *PRL* **97** 053003.
[18] Mårtensson N, Svensson S and Gelius U 1987 *JPB* **20** 6243.
[19] Maurer R J and Watson R L 1986 *Atom. Data Nucl. Data Tab.* **34** 185
[20] http://aphysics2.lanl.gov/cgi-bin/ION/runlanl08d.pl.
[21] Pettersson L *et al* 1982 *J. Electron Spectrosc. Relat. Phenom.* **27** 29.
[22] Svensson S *et al* 1988 *J. Electron Spectrosc. Relat. Phenom.* **47** 327.
[23] Krause M O *et al.* 1970 *Phys. Lett.* **31A** 81.
[24] Rosenzweig J B *et al.* 2008 *Nucl. Instrum. Methods A* **593** 39.